Gap Coupled Dual-Band Petal Shape Patch Antenna for WLAN / WiMAX Applications

Brijesh MISHRA, Vivek SINGH, Rajeev SINGH

Department of Electronics and Communication, Faculty of Science, University of Allahabad, Senate House, University Road, Allahabad, Uttar Pradesh 211002, India

brijesh.mishra0933@gmail.com, vivek.10singh@gmail.com, rsingh68@gmail.com

DOI: 10.15598/aeee.v16i2.2416

Abstract. *A compact gap coupled dual-band patch antenna is proposed for WLAN and WiMAX applications. Two resonating frequencies at 3.6 GHz and 5.2 GHz with a frequency ratio of 1.40 (theoretical), 1.45 (simulated) and 1.48 (measured) are observed. The frequency ratio depends on the thickness of substrate and gap length between the fed and parasitic patches. The impedance bandwidth at lower resonant frequency is 23.7 % (theoretical), 3.9 % (simulated) and 8.7 % (measured) and at upper resonant frequency it is 23.5 % (theoretical), 4 % (simulated) and 9.2 % (measured). Simulated gain of the patch antenna is 1.6 dBi at lower resonant frequency and 4.2 dBi at upper resonant frequency. Voltage Standing Wave Ratio (VSWR) remains below 1.2. The electric and magnetic field radiation patterns at both the resonating frequencies clearly depict that the co-polarization is higher than the cross polarization. Experimental return loss* ($|S_{11}|$)*, VSWR, input impedance and group delay are in close agreement with theoretical and simulated (by High Frequency Structure Simulator (HFSS) Software) results.*

Keywords

Cavity model, circular patch, equivalent circuit, parasitic element, shorting pin, transformed patch.

1. Introduction

Micro-strip antennas with different nomenclature, shape, size and design for various applications are reported in literature [1], [2], [3], [4], [5], [6], [7] and [8]. The shape of the antenna is intuitive however the physical parameters can be altered and optimized to operate in a particular range of frequency. In order to reduce volume, planar area and circuit complexity, two single band antennas were replaced by dual-band micro-strip patch antenna [9]. Recently a dual-band monopole antenna with double spurline for PCS (Personal Communication System) and Bluetooth applications [10], and a miniaturized dual-band antenna for WLAN applications [11] have been reported.

Micro-strip patch antennas have gained special attention in the field of WLAN, Wi-Fi, WiMAX and satellite communications. Numerous designs covering the aforesaid applications and its analysis thereof have been reported [12], [13], [14], [15] and [16].

Some of the inherent drawbacks of the micro-strip antennas are its narrow bandwidth, low gain and low radiation efficiency [17] and [18]. To improve the gain, bandwidth and to make antenna multi-resonating, a number of techniques such as loading of notches and slots of different shape and size on the patch, posting a shorting pin on the radiating patch and introducing a gap between patches are reported [19], [20], [21], [22], [23], [24], [25], [26], [27], [28] and [29]. The purpose of introducing a slot or notch is to reduce overall area of the patch. Further, introduction of a slot and a notch changes the inductive and capacitive behavior of the distributed element and the lumped element equivalent and theoretical analysis becomes more complex. In the present case, we achieve a fairly compact antenna without slot or notch.

Multi-band antenna designs are preferred as they can be easily embedded in MMICs. The researches on some alternative techniques to enhance the bandwidth are going on at a fast pace [30].The antennas reporting improvement in impedance bandwidth by means of different techniques suffer from low gain, poor radiation pattern, and in the absence of theoretical details and/or experimental verification, a proper justification of the obtained results is not possible.

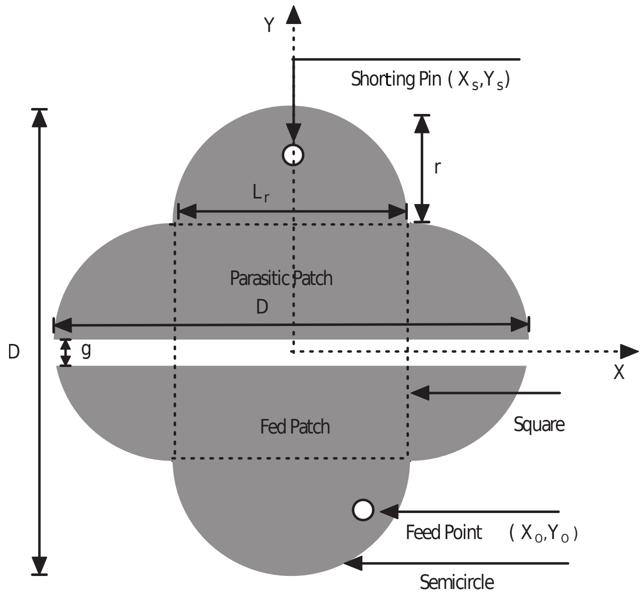

(a) Front view of the geometrical structure of the proposed antenna.

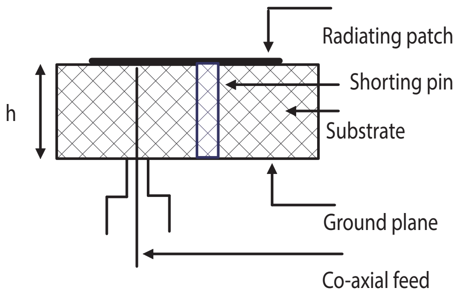

(b) Geometrical side view of the proposed antenna.

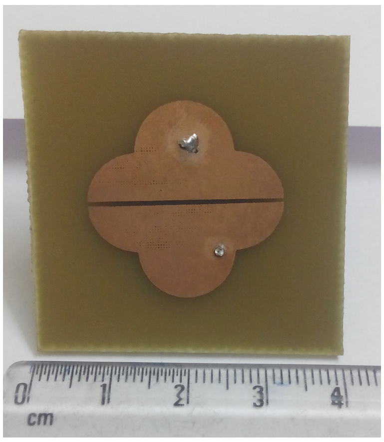

(c) Front view photograph of the fabricated antenna.

Fig. 1: (a) Front view of the geometrical structure of the proposed antenna, (b) geometrical side view of the proposed antenna and (c) front view photograph of the fabricated antenna.

In the present work, the shape of the antenna is conceived and created by combining two different shapes, viz. square and semi-circle. As shown in Fig. 1(a), the square patch (shown by dotted line) is surmounted by the semi-circular patches on each side of the square patch. The entire structure is separated along the x-axis with a gap of 1 mm. Figure 1(a) forms a structure of a gap coupled petal shape antenna. A comparative overview of different antenna structures is presented in terms of patch volume, patch area, substrate material, impedance bandwidth and gain in Tab. 1.

The proposed antenna (cf. Fig. 1) is analyzed using the concepts of cavity model and circuit theory. The parametric analysis has been performed using HFSS software by ANSYS and the simulated results have been validated by experimental and theoretical results. The proposed structure has been simulated and optimized with and without parasitic element. Copper shorting pin is inserted between the ground plane and the radiating patch to enhance the bandwidth and gain of the proposed antenna. We propose an antenna with minimum volume and area as compared to other antennas reported in Tab. 1. A maximum reduction of 91.46 % in volume and 78.2 % in patch area is achieved in the present work as compared to the works reported in references in Tab. 1. The percentage reduction has been calculated taking the volume and patch area of the proposed antenna as reference values.

The antenna is fabricated on a FR-4 epoxy substrate (relative permittivity of substrate ($\epsilon_r = 4.4$) and loss tangent ($\tan\delta = 0.02$)) in the laboratory. The VSWR, return loss ($|S_{11}|$), group delay and input impedance have been experimentally measured by vector network analyzer (VNA) E5071C. The parameters such as VSWR, radiation pattern, antenna gain, frequency ratio and surface current distribution determine the performance of proposed antenna which is presented in the subsequent sections.

2. Antenna Design and Theoretical Analysis

The geometrical top view, side view and the fabricated top view of the proposed micro-strip patch antenna are shown in Fig. 1(a), Fig. 1(b) and Fig. 1(c), respectively. Four semicircles are surmounted on each side of a square patch creating a petal shape and a rectangular ($D \times g$) mm^2 slot is removed from the patch along the x-axis to divide it into two parts, one being a fed patch and other being a parasitic patch, resulting into the proposed antenna. The patch placed close to the fed or driven patch gets energized through the suitable radiating coupling is termed as parasitic patch. Equivalent T or π circuit represents an arbitrary discontinuity at the junction of two patches [36] as shown in Fig. 2(a) and Fig. 2(b). The radiating patch antenna has been excited by the 50 Ω coaxial connector. Design

Tab. 1: An overview of antenna shape, volume, patch area, resonating frequency, impedance bandwidth and gain.

References	Antenna shape/sub-strate	Patch volume [mm^3]	Patch area [mm^2]	Increment in patch volume [%] / area from reference value	Resonating frequency (Lf/Hf) [GHz]	Impedance bandwidth at LB/HB [%]	Antenna gain at (Lf/Hf) [dBi]
[19]	W-shape/RT Duroid & Foam	4800	1200	80.8/52	4.17/5.78	5.28/2.77 (T)	9.06/4.18 (S)
[31]	H-shape/Foam & Air	2944	736	68.69/21.73	2.4/5	4.8/3.8 (S)	2.75/3.9 (S)
[32]	V-shape / FR4-epoxy	10800	2400	91.46/76	2.4 (SB)	3.2 (M)	NR
[33]	E-shape/TMM4	4107.5	2650	77.56/78.2	3.1/7.2	3.9/7.5 (M)	4.6/4 (M)
[34]	L-shape-strip / ($\epsilon_r = 3.5$)	2280	1520	59.57/62.1	2.4/5	16.9/32.9 (M)	-0.4/1.8 (M)
[35]	F-shape / FR4-epoxy	42240	1400	58.85/58.9	2.44/5.18	26.8/11.4 (S)	2/2.89 (S)
Proposed	Petal-shape / FR4-epoxy	921.6	576	Reference value (volume/area) 921 mm^3 / 576 mm^2	3.6/5.2	8.7/9.2 (M)	1.6/4.2 (S)
Legends: TMM4 - Thermoset Microwave Material, Lf - Lower Resonating Frequency, Hf - Higher Resonating Frequency, S - Simulated, M - Measured, T - Theoretical, NR - Not Reported, LB - Lower Frequency Band, HB - Higher Frequency Band, SB - Single Band							

specifications of the proposed antenna are tabulated in Tab. 2.

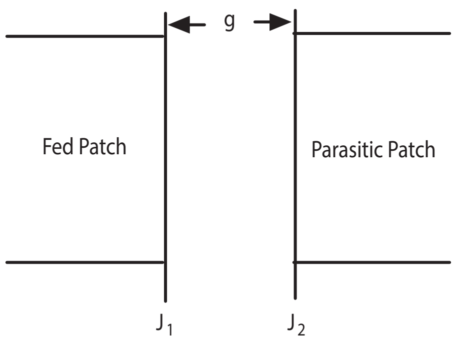

(a) Physical structure of gap between two patches.

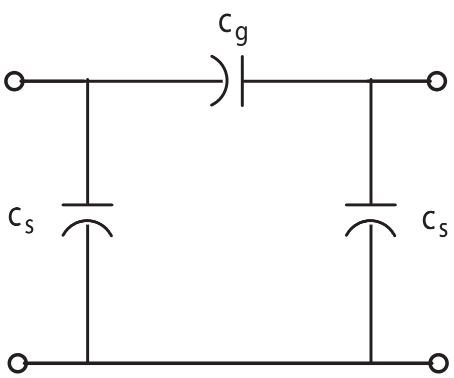

(b) Equivalent circuit of gap between two patches.

Fig. 2: (a) Physical structure of gap and (b) equivalent circuit of gap between two patches.

Tab. 2: Design specifications of the proposed petal shape antenna.

Design specifications	Values
Dimension of patch ($D \times D$)	(24×24) mm^2
Side length of square patch (L_r)	12 mm
Radius of semicircle (r)	6 mm
Gap between fed and parasitic patch (g)	0.5 mm
Feed point (X_0, Y_0)	(4, −6) mm
Radius of shorting pin	1 mm
Location of shorting pin (X_s, Y_s)	(0, 8) mm
Reference point	(0, 0) mm
Thickness of substrate (h)	1.6 mm
Width of rectangular portion - 2&4 (W_r)	5.75 mm
Width of rectangular portion - 3 (W_c)	2.65 mm
Width of the transformed rectangular patch (W_p)	8.4 mm
Length of transformed rectangular patch portion -2&4 (L_c)	4.66 mm
Length of transformed rectangular patch (L_p)	21.32 mm

The rectangular $(L_p \times W_p)$ mm^2 micro-strip patch antenna is viewed as a parallel combination of resistance (R), inductance (L) and capacitance (C). The values of these elements can be calculated according to [37]:

$$C = \frac{L_p W_p \epsilon_0 \epsilon_e}{2h} \cos^{-2}\left(\frac{\pi X_0}{L_p}\right), \tag{1}$$

$$R = \frac{Q}{\omega_r C}, \tag{2}$$

$$L = \frac{1}{\omega_r^2 C}, \tag{3}$$

where h is thickness of the substrate, X_0 is X-coordinates of feed foint, $f_r = \frac{c}{2L_p\sqrt{\epsilon_e}}$, f_r is resonating frequency is related to $\omega_r = 2\pi f_r$,

$$Q = \frac{c\sqrt{\epsilon_e}}{4f_r h}. \tag{4}$$

In Eq. (4), c is the velocity of light in m·s^{-1}, Q is the quality factor, ϵ_0 is the permittivity of free space, ϵ_e is effective permittivity for $W_p/h \geq 1$ and ϵ_r is the relative permittivity of the substrate material. The effective permittivity is given according to [38]:

$$\epsilon_e = \frac{\epsilon_r + 1}{2} + \frac{\epsilon_r - 1}{2}\left(1 + \frac{10h}{W_p}\right)^{-\frac{1}{2}}. \tag{5}$$

The antenna comprises of two identical (fed and parasitic) resonating patches by proper adjustment of gap 'g' between them. It has been already reported [38] that a semi-circular disc can be transformed and made equivalent to a rectangular patch. The proposed antenna is transformed to its equivalent rectangular patches as shown in Fig. 3, for simplifying mathematical analysis. Equivalent circuits of the transformed driven and the parasitic patches are shown in Fig. 4(a) and Fig. 4(b), respectively. Physical dimensions of both the patches are same due to their symmetrical structure. Therefore, the equivalent circuits, as well as their elemental values, are same. Dimensions of transformed equivalent rectangular patches are deduced in the following manner:

In Fig. 3(a), area of each half semi-circular patch portion-2 and 4 and the area of the removed portion below the patch portion-2 and 4 is equal to $\frac{1}{4}\pi r^2$ and $\frac{g}{2}r$ respectively. The resultant area (A) of the patch portion-2 and 4, therefore, is given by

$$\frac{1}{4}\pi r^2 - \frac{g}{2}r. \tag{6}$$

The area (A) of the transformed equivalent rectangular patch portion-2 and 4 (cf. Fig. 3(b)) is equal to

$$A = L_c \times W_r = \frac{1}{4}\pi r^2 - \frac{g}{2}r, \tag{7}$$

where $W_r = r - \frac{g}{2}$ is the transformed width and L_c is the transformed length of the rectangular patch portion-2 and 4 (for both fed and parasitic patch). The semi-circular patch portion-3 is also transformed to its equivalent rectangular patch and the area is given as

$$A = L_p \times W_c = \frac{1}{2}\pi r^2, \tag{8}$$

where L_p is the transformed patch length and W_c is the width of the rectangular patch of semicircular portion-3 (for both fed and parasitic patch). The proposed

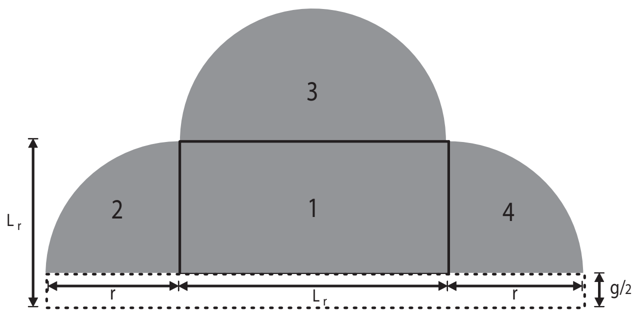

(a) Half portion of the proposed antenna.

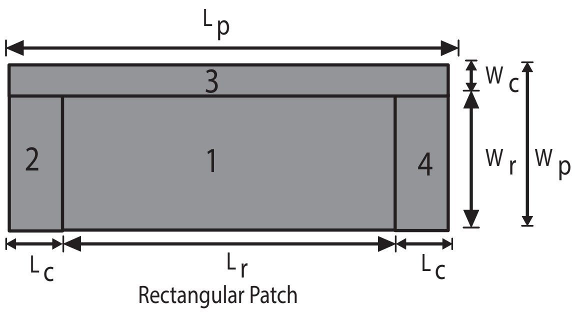

(b) Transformed equivalent rectangular patch of the structure of Fig. 3(a).

Fig. 3: (a) Half portion of the proposed antenna and (b) transformed equivalent rectangular patch of the structure.

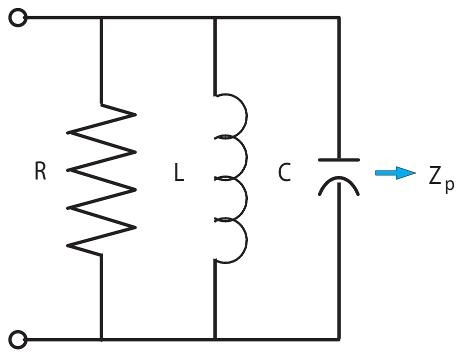

(a) Equivalent circuit of feed patch.

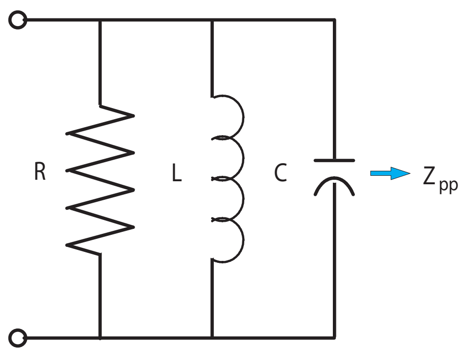

(b) Equivalent circuit of parasitic patch.

Fig. 4: Equivalent circuit of (a) feed patch and (b) parasitic patch.

petal shaped patch antenna is transformed into two equivalent rectangular patches ($L_p \times W_c$) separated by a gap (g), where $L_p = [L_r + 2L_c]$, and $W_p = W_r + W_c$. Values of W_p, W_r, W_c and L_p, L_r, L_c are tabulated in Tab. 2.

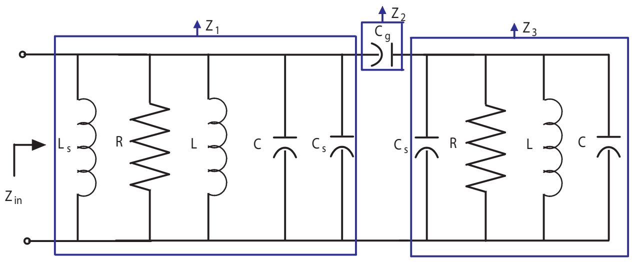

(a) Equivalent circuit diagram of the proposed antenna.

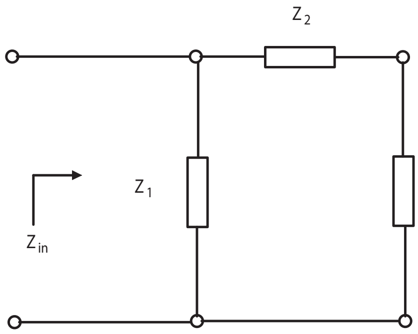

(b) Modified equivalent circuit of Fig. 5(a).

Fig. 5: Equivalent circuit diagram of the (a) proposed antenna and (b) modified equivalent circuit.

The equivalent circuit and modified equivalent circuit of proposed antenna are shown in Fig. 5(a) and Fig. 5(b) respectively. The expression of gap capacitance C_g and plate capacitance C_s of the micro-strip patch are calculated according to [39]:

$$C_g = 0.5hQ_1 e^{-1.86\frac{g}{h}} \left(1 + 4.09\left(1 - e^{0.75\sqrt{\frac{h}{W_p}}}\right)\right), \quad (9)$$

$$C_s = C_L \left(\frac{Q_2 + Q_3}{Q_2 + 1}\right), \quad (10)$$

where

$$Q_1 = 0.04598\left(0.03 + \left(\frac{W_p}{h}\right)^{Q_4}\right)(0.272 + 0.07\epsilon_r), \quad (11)$$

$$Q_2 = 0.107\left(\frac{W_p}{h} + 9\right)\left(\frac{g}{h}\right)^{3.23} + + 2.09\left(\frac{g}{h}\right)^{1.05}\left(\frac{1.5 + 0.3\left(\frac{W_p}{h}\right)}{1 + 0.6\left(\frac{W_p}{h}\right)}\right), \quad (12)$$

$$Q_3 = e^{-0.5978} - 0.55, \quad (13)$$

$$Q_4 = 1.23, \quad (14)$$

C_L is the terminal capacitance of the open circuited conductor, given by

$$C_L = C_{ll}\frac{\sqrt{\epsilon_e}}{Z_0 C}, \quad (15)$$

where C_{ll} is the conductor extension length:

$$C_{ll} = 0.412h\frac{(\epsilon_e + 0.3)\left(\frac{W_p}{h} + 0.264\right)}{(\epsilon_e - 0.258)\left(\frac{W_p}{h} + 0.8\right)}, \quad (16)$$

Z_0 - characteristic impedance.

Also the input impedance of the proposed antenna of Fig. 5(b) can be given as:

$$Z_{in} = \frac{Z_1(Z_2 + Z_3)}{Z_1 + Z_2 + Z_3}, \quad (17)$$

where:

$$Z_1 = \frac{1}{\frac{1}{j\omega L_s} + \frac{1}{Z_p} + j\omega C_s}. \quad (18)$$

By introducing the shorting pin on the patch, a parallel inductance L_s is added to the whole patch and the equivalent circuit is modified for the proposed antenna as shown in Fig. 5(a). The inductance value of shorting pin is calculated after [40] and is given by Eq. (19):

$$L_s = \frac{\eta_0 W_p L_p}{2\pi c}\ln\left(\frac{4c}{EW_p d\sqrt{\epsilon_r}}\right), \quad (19)$$

where: d is diameter of the shorting pin, E is Euler's constant $= 0.5772$, $\eta_0 = 120\pi$.

Z_2 and Z_3 as shown in Fig. 5(b) are given by the following:

$$Z_2 = \frac{1}{j\omega C_g}, \quad (20)$$

$$Z_3 = \frac{1}{\frac{1}{Z_{pp}} + j\omega C_s}. \quad (21)$$

Z_p is the impedance of fed patch (cf. Eq. (18) and Eq. (21)) while Z_{pp} is the impedance of parasitic patch and are given as:

$$Z_p = Z_{pp} = \frac{1}{\frac{1}{R} + j\omega C + \frac{1}{j\omega L}}. \quad (22)$$

Using the above-mentioned equations, the total input impedance of the proposed antenna is calculated and the other antenna parameters such as reflection coefficient, VSWR and return loss are:

Reflection coefficient $(\gamma) = \dfrac{Z_0 - Z_{in}}{Z_0 + Z_{in}}$;

and VSWR $= \dfrac{1 + |\gamma|}{1 - |\gamma|}$;

the Return Loss (RL) $= -20\log|\gamma|$.

3. Results and Discussion

The distributed surface current density for the proposed gap coupled patch antenna at the lower (3.6 GHz) and upper (5.2 GHz) resonating frequencies, respectively are shown in Fig. 6(a) and Fig. 6(b). It has been observed that at lower resonant frequency, the parasitic patch is energized by the driven patch and maximum current is flowing from right to left along the coupled edge. Parasitic patch is radiating at a lower resonant frequency only, whereas at upper resonating frequency only the driven patch is radiating. Maximum current is flowing along the left and the right edges of the fed patch at higher frequency along with the y-axis. Surface current density and the current direction observed at resonating frequency of 3.6 GHz (cf. Fig. 6(a)), suggest [17] that the dominant mode is TM_{10}. Similarly, at resonating frequency of 5.2 GHz (cf. Fig. 6(b)) the current direction indicates that the dominant mode is TM_{20} [17].

On observation of the results of Fig. 10 and Fig. 6(a), we infer that the lower resonating frequency (3.6 GHz) remains unchanged with the variation of gap length g and a maximum simulated surface current distribution is observed as 209 $A{\cdot}m^{-1}$. With the change in the gap length, the lower resonating frequency is marginally shifting (cf. Fig. 10), therefore, the dominant mode (TM_{10}) for all the gap lengths will remain unchanged.

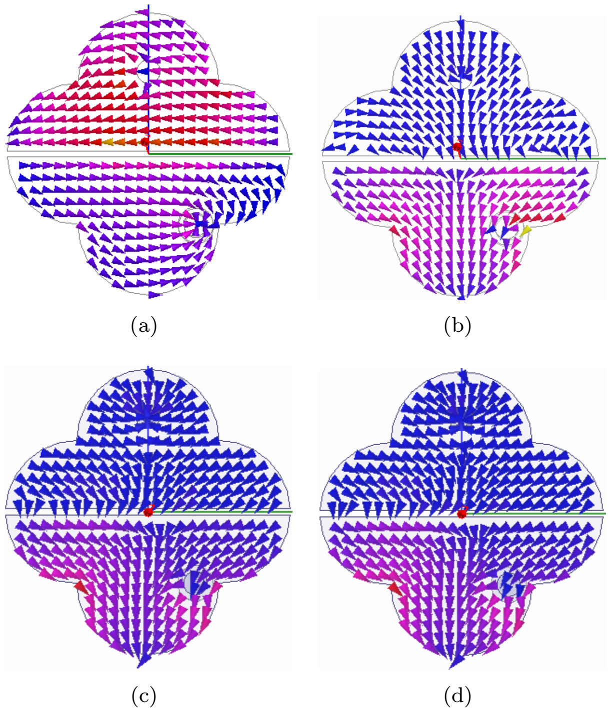

Fig. 6: Current distribution of proposed antenna at (a) 3.6 GHz ($g = 0.5$ mm), (b) 5.2 GHz ($g = 0.5$ mm), (c) 5.3 GHz ($g = 1$ mm) and (d) 5.3 GHz ($g = 1.5$ mm).

With the increment of 0.5 mm in gap length (from 0.5 mm to 1.0 mm and from 1.0 mm to 1.5 mm) we observe an increasing shift of 100 MHz / 0.5 mm (cf. Fig. 10) in the resonating frequency. On perusal of current distribution diagrams Fig. 6(b), Fig. 6(c) and Fig. 6(d), it is evident that the maximum surface current densities (shown as red in Fig. 6) are 120 $A{\cdot}m^{-1}$ (for $g = 0.5$ mm, f_r is 5.2 GHz), 170 $A{\cdot}m^{-1}$ (for $g = 1.0$ mm, f_r is 5.3 GHz), 178 $A{\cdot}m^{-1}$ (for $g = 1.5$ mm, f_r is 5.4 GHz). With the change in gap length and resonant frequencies, we observe a change in magnitude of the current density but no change is observed in the direction of the current, hence, it can be safely concluded that the dominant mode is TM_{20} [17].

Theoretical (3.46 GHz), simulated (3.59 GHz) and measured (3.60 GHz) lower resonant frequencies and theoretical (5.10 GHz), simulated (5.22 GHz) and measured (5.34 GHz) upper resonant frequencies are reasonably in close agreement as inferred from plot of return loss versus frequency (cf. Fig. 7).

A large impedance bandwidth with good return loss is desirable for an efficient transmission/reception of the signal in the given frequency band. A monotonically increasing behavior of impedance bandwidth is observed in Fig. 8. Impedance bandwidths (at -10 dB $|S_{11}|$) at lower resonant frequencies are 23.7 % (theoretical), 3.9 % (simulated) and 8.7 % (measured) and at upper resonant frequencies are 23.5 % (theoretical), 4 % (simulated) and 9.2 % (measured) are observed.

By conserving the area, petal shape geometry is transformed to its rectangular equivalent. A lumped element equivalent circuit obtained from the distributive transformed rectangular element is shown in Fig. 5(a) and Fig. 5(b). Theoretical analysis of the lumped el-

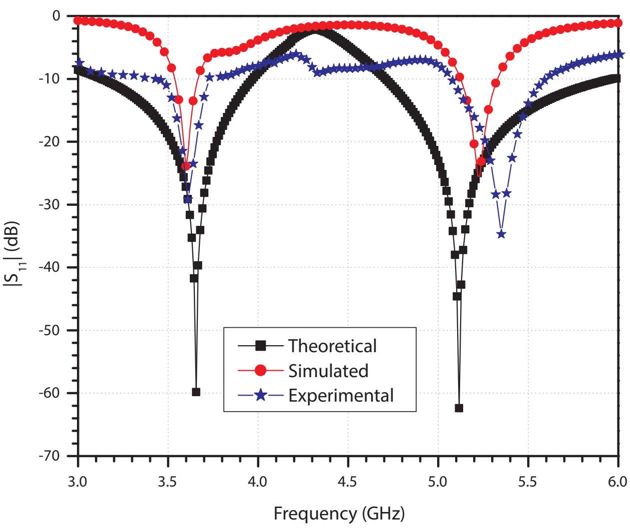

Fig. 7: Theoretical, simulated and measured return $|S_{11}|$ loss versus frequency.

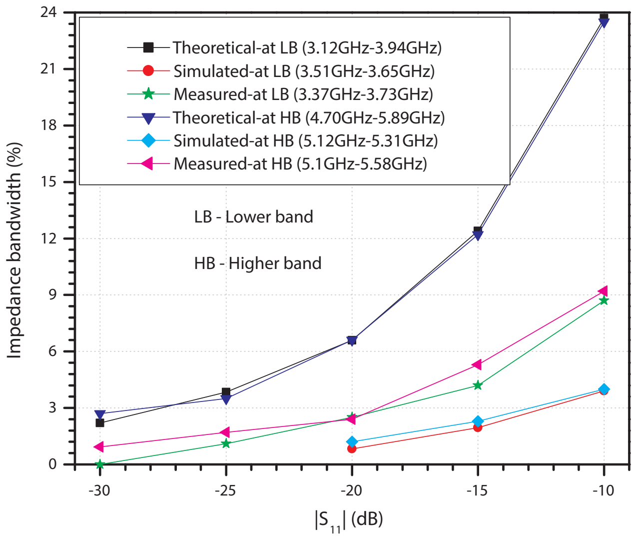

Fig. 8: Theoretical, simulated and measured impedance bandwidth as a function of $|S_{11}|$.

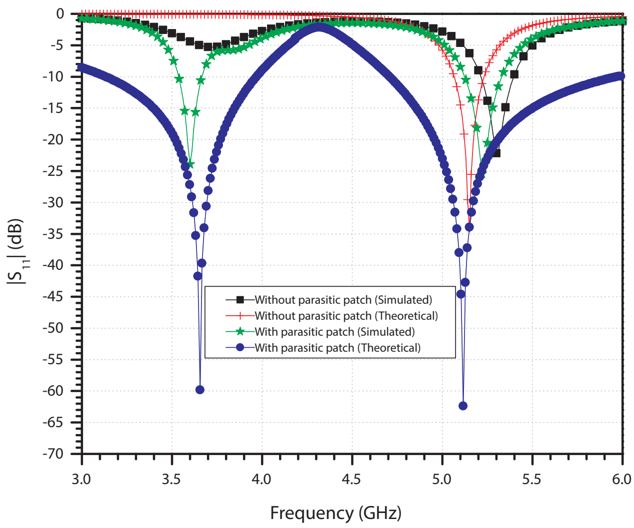

Fig. 9: Simulated and theoretical return loss $|S_{11}|$ of with and without parasitic patch antenna.

ement circuit (cf. Fig. 5(a) and Fig. 5(b)) is shown in Fig. 7 and Fig. 8. A significant difference between the simulated and theoretical, measured and theoretical bandwidths is observed from Fig. 7 and Fig. 8. The reason of this difference is attributed to the difference in shape and size of the rectangular and petal shape patches. As only the area in the transformed rectangular patch is conserved, both the patches (rectangular and petal shape) produce different current distribution patterns, this causes the other antenna parameters like impedance bandwidth, radiation pattern, gain and radiation efficiency to vary with shape and size.

On the basis of above discussion, it can be safely concluded that it is not possible to compare the different antenna parameters obtained by means of theoretical analysis of lumped element circuit and obtained by simulation of actual antenna structure or experimentally. The return loss plot obtained from theoretical analysis (transformed patch analysis) is used to validate only the resonant frequencies of the designed structure [41]. Further, assumptions involved in theoretical analysis fail to correctly predict all other antenna parameters (except resonant frequency) including bandwidth [38] and [40].

We report a better impedance bandwidth in the present work (8.7/9.2 %) than antenna with H-shape (4.8/3.8 %), W-shape (5.28/2.77 %), V-shape (3.2 %), E-shape (3.9/7.5 %) and less than L-shape (16.9/32.9 %) and F-shape (26.8/11.4 %). However, the L-shape and F-shape antennas occupy a larger volume of 59.57 % and 58.85 % and patch areas of 62.1 % and 58.9 % respectively as compared to the proposed antenna. The large impedance bandwidth in L-shape and F-shape antennas is due to use of micro-strip line as feed line.

A single band is observed in case of the fed patch only, i.e. without parasitic patch, whereas for the proposed structure, i.e. with parasitic patch, two resonating frequencies are observed (cf. Fig. 9). Current distribution in parasitic patch is responsible for the presence of lower resonating frequency and is confirmed by the observation of theoretical and simulated return loss curve for antenna with parasitic patch (cf. Fig. 9). The result observed in the Fig. 9 is in conformity with the other reported results for structures having only fed patch, i.e. without parasitic patch and with parasitic patch [38].

Effect of gap length g is depicted in Fig. 10 by means of return loss versus frequency variation. A marginal change is observed at the lower resonating frequencies as the gap length is increased whereas with the in-

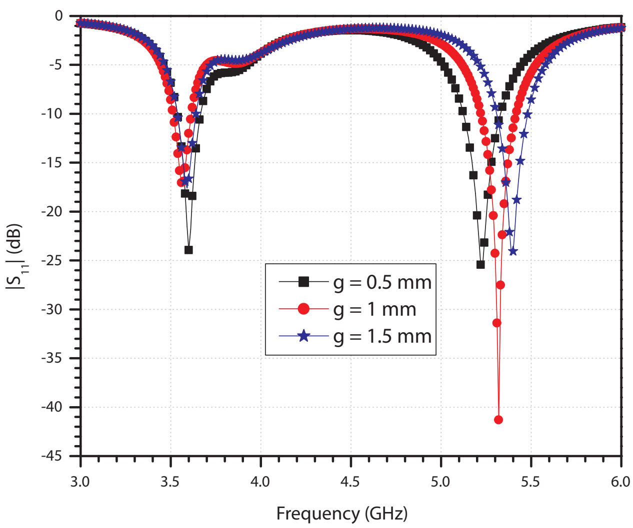

Fig. 10: Variations of return loss $|S_{11}|$ with frequency for different values of gap g.

crease in the gap length we observe (cf. Fig. 10) a shift in resonant frequency. The reason for shift in resonating frequency is because the total gap capacitance is the function of the gap length (cf. Eq. (9), Eq. (10), Eq. (11), Eq. (12), Eq. (13), Eq. (14), Eq. (15) and Eq. (16)), which changes exponentially with change in resonating frequency. An optimal gap length of 0.5mm is chosen so that the patch area of the antenna remains conserved and exponential shift of resonating frequency at higher frequencies can be avoided.

The variation of return loss with frequency for different values of substrate thickness h in the case of the proposed antenna is shown in Fig. 11. Antenna return loss behavior with substrate heights $h = 0.6$ mm, 1.6 mm and 2.6 mm are simulated. FR-4 glass epoxy substrate with a height of 1.6 mm is chosen for prototype as it is easily and commercially available. Further, as the height of the antenna is increased (from 1.6 mm to 2.6 mm), the overall volume will increase (by 62.5 %) which will make the antenna unsuitable to be embedded in sleek and small devices. While when the height of the substrate is reduced (from $h = 1.6$ mm to 0.6 mm), the return loss is not sufficient and it resonates only at a single frequency (5.4 GHz) making the antenna unsuitable for the desired application. For $h = 2.6$ mm a marginal shift towards a lower frequency region at lower resonating frequency and a shift of approximately 210 MHz towards the lower frequency region of higher resonating frequency is observed from the reference substrate height ($h = 1.6$ mm). Increment and decrement in the height of the substrate affects the capacitance C (Eq. (1)), i.e. C decreases with increase in height h which in turn increases R and L, this alters the total operating frequency of the antenna. Further, the alteration in substrate height shifts the impedance loci and is the reason for the shift in resonant frequency.

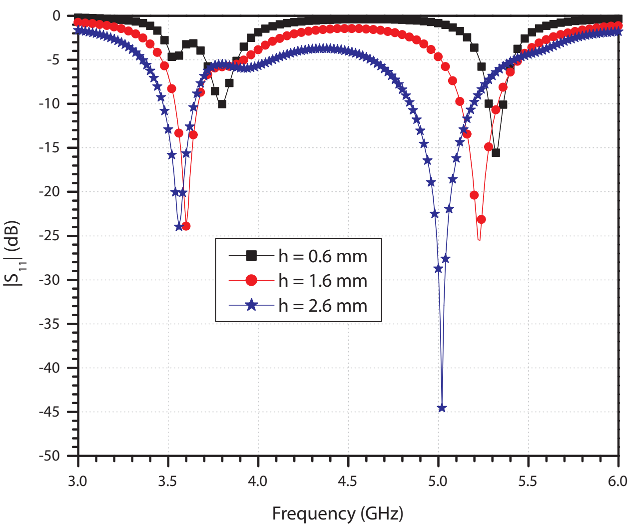

Fig. 11: Return loss $|S_{11}|$ versus frequency plot for different values of substrate (FR-4) thickness h.

As observed in Fig. 12, frequency ratio varies with the change in substrate height and gap length. For the proposed antenna the gap length is 0.5 mm, substrate height is 1.6 mm, and the simulated frequency ratio is 1.45. Increase in gap length increases the frequency ratio, whereas a similar behaviour is not observed when the substrate height is increased. A percentage difference of 2.6 % between experimental and simulated frequency ratio, 3.4 % between simulated and theoretical frequency ratio and 6.0 % between experimental and theoretical frequency ratio is observed. Percentage difference between simulated and experimental frequency ratio is well within the permissible limits of error. As discussed above due to the difference in shape and size of the simulated and theoretical structures a percentage difference of 6 % in frequency ratio is observed.

A simulated gain of an antenna with shorting pin, without shorting pin and without parasitic patch is il-

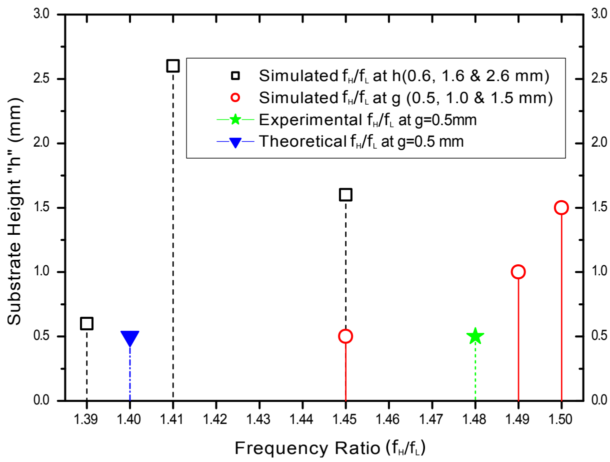

Fig. 12: Variation of frequency ratio with gap length and substrate height.

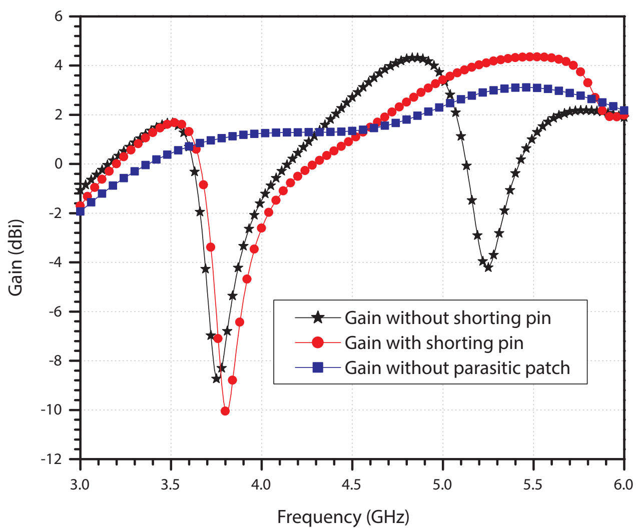

Fig. 13: Gain versus frequency plot with and without shorting pin on the patch.

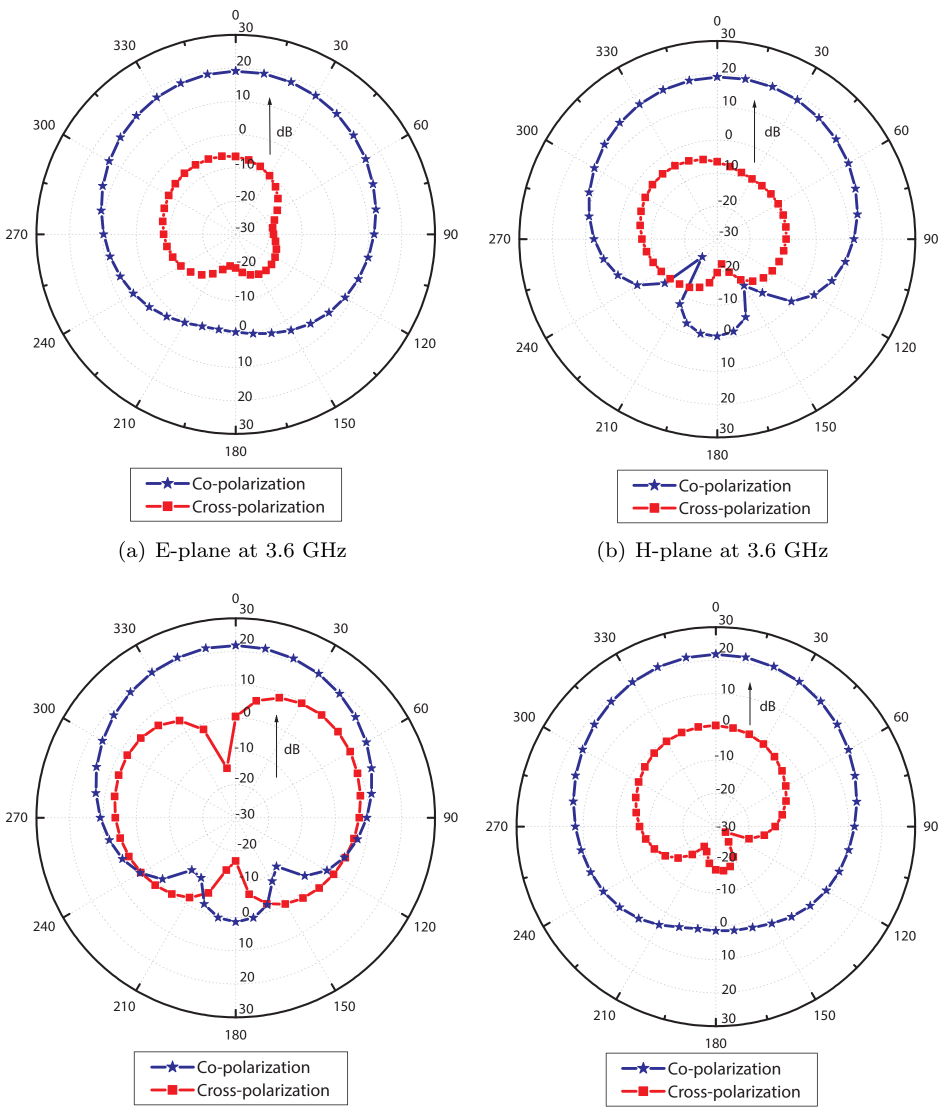

(a) E-plane at 3.6 GHz (b) H-plane at 3.6 GHz

(c) E-plane at 5.2 GHz (d) H-plane at 5.2 GHz

Fig. 14: Simulated radiation pattern.

lustrated in Fig. 13. After inserting the shorting pin on the parasitic patch it is observed that the gain remains constant (1.6 dBi) at the lower resonating frequency while gain is increased from -4 dBi to 4.2 dBi at upper resonant frequency. For a shorted antenna we observe an enhanced gain as compared to the antenna without parasitic patch. In the present work, we report a better-simulated antenna gain (4.2 dBi) at higher resonating frequency than antennas with H-shape (3.9 dBi) and F-shape (2.89 dBi). The gain of the W-shape antenna at higher resonating frequency is equal to the antenna gain obtained in the present work. The reason of better antenna gain at lower resonating frequencies for H-shape and W-shape is attributed due to the substrate material (foam for H-shape and RT Duroid and foam for W-shape) and height (4 mm both for H-shape and W-shape antennas) of the substrate. The resonant frequency changes with the change in the substrate material and its height. It is well established that the gain increases as the height of the substrate increases.

Radiation pattern (co-polarization and cross-polarization) in the XZ-plane ($\varphi = 0°$, E-plane) and YZ-plane ($\varphi = 90°$, H-plane) of the proposed antenna for both the resonating frequencies is observed in Fig. 14. There is sufficient difference between co-polarization level and cross-polarization level (in dB) in both E-plane as well as H-plane. The radiation pattern in E-plane for 3.6 GHz and H-plane for 5.2 GHz shows omni-directional behavior while good broadside radiation pattern behavior is observed in H-plane for 3.6 GHz and E-plane for 5.2 GHz with desirable low cross-polarization levels.

Theoretical, simulated and measured plot of VSWR versus frequency is shown in Fig. 15. A VSWR less than 1.2 is observed in each case which is suggestive of good impedance matching.

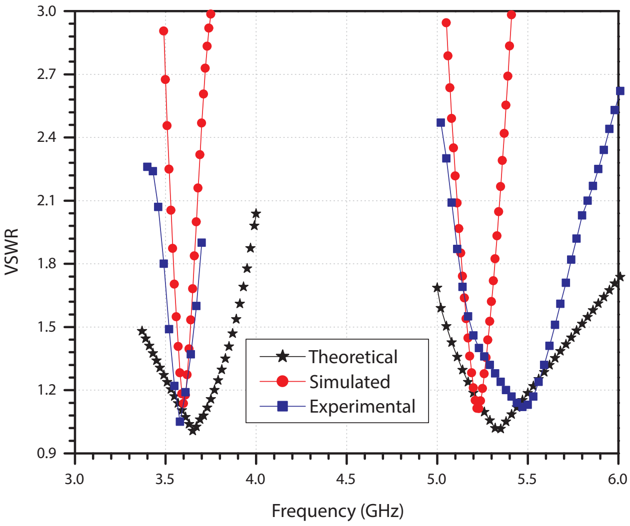

Fig. 15: Theoretical, simulated and measured VSWR.

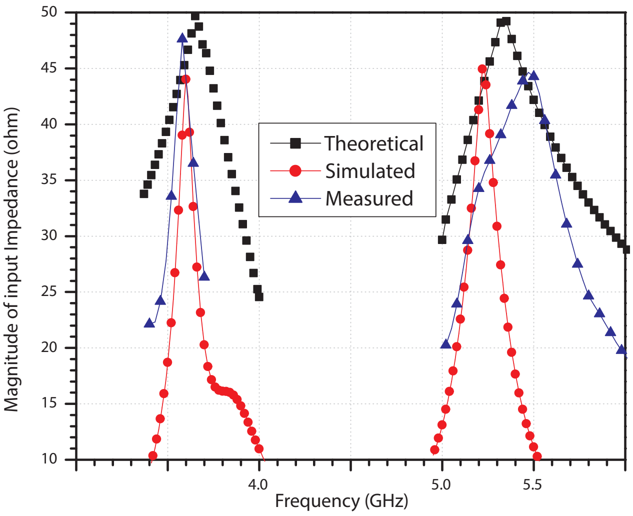

Fig. 16: Theoretical, simulated and measured input impedance $|Z_{in}|$.

The antenna is excited by a coaxial probe feed of 50 Ω characteristic impedance. To excite the patch on a given frequency, impedance matching (impedance of the antenna is same as characteristics impedance) is required between the patch and connector at the given frequency. Theoretical, simulated and experimental input impedance values are presented in Fig. 16. At lower resonant frequencies the input impedances are 50 Ω (theoretical), 47.9 Ω (simulated) and 44.3 Ω (experimental) while at higher resonant frequencies input impedances are 49.3 Ω (theoretical), 45.1 Ω (simulated) and 34.5 Ω (experimental). Similar nature of curves is observed in case of theoretical, simulated and measured VSWR and input impedances (cf. Fig. 15 and Fig. 16). This indicates that the theoretical, simulated and experimental resonating frequencies can be correctly predicted with small change in impedance and VSWR. However, it is difficult to predict other antenna parameters theoretically.

The overall radiating mechanism of the patch antenna is least affected by the marginal shift in the lower and upper resonating frequencies and is established by the fact that the nature of theoretical, simulated and experimental curves is similar (cf. Fig. 7, Fig. 9, Fig. 11, Fig. 15 and Fig. 16).

The marginal impedance mismatch is caused due to approximation in calculations, mathematical instability involved in parameter calculation by the software, introduction of fringe capacitance and mechanical tolerances in the fabrication of prototype antenna. The least count errors of the measuring instruments are also the cause of variation in measured and simulated values.

A marginal variation between theoretical, simulated and measured lower resonating frequencies is observed in Fig. 15 and Fig. 16. The percentage variation between theoretical, simulated and measured lower resonating frequencies (cf. Fig. 15 and Fig. 16) is similar to the variation observed in Fig. 7. A more pronounced variation between theoretical, simulated and measured higher resonating frequencies is observed in Fig. 15 and Fig. 16 which are similar to that of the variation observed in Fig. 7. VSWR and return loss measurements provide the similar nature of information and the same is established by the observation of Fig. 7 and Fig. 15. Resonant frequencies as observed from Fig. 7, Fig. 15 and Fig. 16 are confirmed from these measurements and all the results validate each other.

As reported recently [29], less than 0.5 ns of group delay variation is desirable for efficient transmitting antenna. Identical or symmetrical patches exhibit good group delay response. As shown in the Fig. 1(a), the fed patch and parasitic patch are identical. Therefore, a good group delay response is expected and informs about the degree of distortion in transmitted/received pulses [42].

Figure 17 depicts the group delay response of the proposed antenna and it is observed that the simulated and measured group delay variation for proposed antennas is less than 0.5 ns for the entire frequency range.

Percentage radiation efficiency of antenna with and without parasitic patch is illustrated in Fig. 18. More than 70 % radiation efficiency is observed for both the antennas. Enhanced efficiency of 9.74 % (3.6 GHz) and 6 % (5.2 GHz) in the case of antenna with parasitic patch is observed as compared to antenna without parasitic patch.

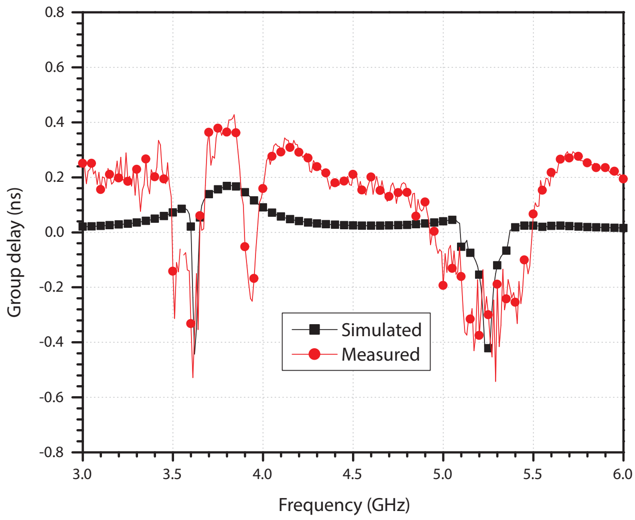

Fig. 17: Group delay response of the proposed antenna.

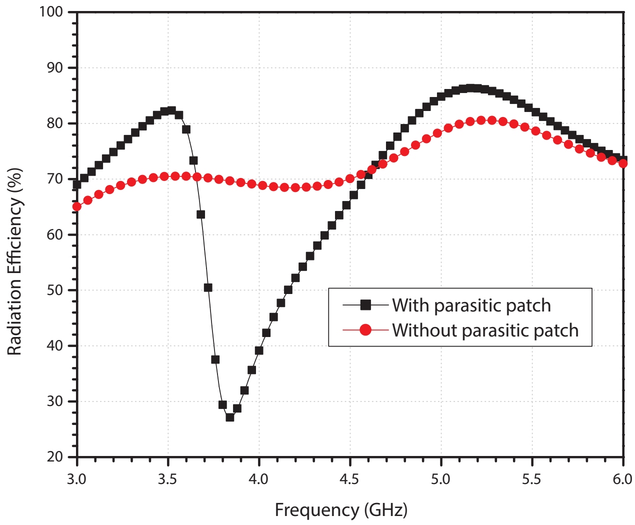

Fig. 18: Radiation efficiency of antenna as a function of frequency.

4. Conclusion

In the proposed antenna structure, we observe a fairly large reduction in overall patch volume and area with an enhanced impedance bandwidth as compared to other reported antennas of H, V, W and E-shapes. The frequency ratio of antenna is sensitive to the change in gap length between parasitic and fed patch and it varies proportionally with gap length. Change in gap length does not affect the lower resonant frequencies whereas we observe at frequency shift of 100 MHz towards higher side with every 0.5 mm increase in gap length. Adding the shorting pin into the parasitic patch, a dual-band (3.6/5.2 GHz) operation and enhancement in overall gain is observed. The low cross-polarization levels in both E-plane and H-plane make the structure suitable for dual-band operation for wireless applications such as WLAN/WiMAX.

References

[1] AYDIN, C., D. C. ATILLA, R. KOPRU, S. KILINC, C. KARAKUS and B. S. YARMAN. A design technique of 50 Ω terminated bandpass matching network and its implementation to a Y-shaped monopole antenna matching. *Analog Integrated Circuits and Signal Processing*. 2016, vol. 89, iss. 3, pp. 665–673. ISSN 1573-1979. DOI: 10.1007/s10470-016-0768-3.

[2] TONG, M.-S., M. YANG., Y. CHEN and R. MITTRA. Finite-difference time-domain analysis of a stacked dual-frequency microstrip planar inverted-F antenna for mobile telephone handsets. *IEEE Transactions on Antennas and Propagation*. 2001, vol. 49, iss. 3, pp. 367–376. ISSN 1558-2221. DOI: 10.1109/8.918610.

[3] NAIDU, P. V. and A. MALHOTRA. A small ACS-fed tri-band antenna employing C and L shaped radiating branches for LTE/WLAN/WiMAX/ITU wireless communication applications. *Analog Integrated Circuits and Signal Processing*. 2015, vol. 85, iss. 3, pp. 489–496. ISSN 1573-1979. DOI: 10.1007/s10470-015-0637-5.

[4] WANG, C.-J., J.-J. LEE and R.-B. HUANG. Experimental studies of miniaturized CPW fed slot antenna with the dual frequency operation. *IEEE Antennas and Wireless Propagation Letters*. 2003, vol. 2, iss. 1, pp. 151–154. ISSN 1548-5757. DOI: 10.1109/LAWP.2003.817578.

[5] KIM, H.-Y., Y.-A. LEE, C.-H. WON and H.-M. LEE. Design of compact dual-band micro-strip patch antenna for GPS/K-PCS operation. In: *Antennas and Propagation Society International Symposium*. Monterey: IEEE, 2004, pp. 3529–3532. ISBN 0-7803-8302-8. DOI: 10.1109/APS.2004.1330107.

[6] PIOCH, S. and J.-M. LAHEURTE. Low profile dual-band antenna based on a stacked configuration of EBG and plain patches. *Microwave and Optical Technology Letters*. 2005, vol. 44, iss. 3, pp. 207–209. ISSN 1098-2760. DOI: 10.1002/mop.20589.

[7] LEE, J. N., J. H. KIM, J. K. PARK and J. S. KIM. Design of dual-band antenna with U-shaped open stub for WLAN/UWB applications. *Microwave and Optical Technology Letters*. 2009, vol. 51, iss. 2, pp. 284–289. ISSN 1098-2760. DOI: 10.1002/mop.24033.

[8] THOMAS, K. G. and M. SREENIVASAN. Compact CPW-fed dual-band antenna. *Electronics*

Letters. 2010, vol. 46, iss. 1, pp. 13–14. ISSN 0013-5194. DOI: 10.1049/el.2010.1729.

[9] MACI, S. and G. B. GENTILI. Dual-frequency patch antennas. *IEEE Antennas and Propagation Magazine*. 1997, vol. 39, iss. 6, pp. 13–20. ISSN 1045-9243. DOI: 10.1109/74.646798.

[10] ANGKAWISITTPAN, N. and A. SIRITARATIWAT. A dual frequency monopole antenna with double spurlines for PCS and bluetooth applications. *Applied Computational Electromagnetic Society*. 2016, vol. 31, iss. 8, pp. 976–981. ISSN 1054-4887.

[11] JIACHEN, Y., H. WANG, Z. LV and H. WANG. Design of Miniaturized Dual-Band Microstrip Antenna for WLAN Application. *Sensors*. 2016, vol. 16, iss. 7, pp. 2–15. ISSN 1424-8220. DOI: 10.3390/s16070983.

[12] BHARTIA, P., K. V. S. RAO and R. S. TOMAR. *Millimeter-wave microstrip and printed circuit antennas*. Norwood: Artech House, 1991. ISBN 978-0890063330.

[13] POZAR, D. M. and D. H. SCHUBERT. *Microstrip antennas, the analysis and design of microstrip antennas and arrays*. New York: IEEE Press, 1995. ISBN 0-7803-1078-0.

[14] GAO, S. and S. ZHONG. Analysis and design of dual polarized microstrip antenna array. *International Journal of RF and Microwave*. 1999, vol. 9, iss. 1, pp. 42–48. ISSN 1099-047X. DOI: 10.1002/(SICI)1099-047X(199901)9:1<42::AID-MMCE6>3.0.CO;2-J.

[15] AHSAN, M. R., M. T. ISLAM, M. H. ULLAH, M. F. MANSOR and N. MISRAN. Dual band printed patch antenna on ceramic–polytetrafluoroethylene composite material substrate for GPS and WLAN applications. *Telecommunication Systems*. 2016, vol. 62, iss. 4, pp. 747–756. ISSN 1572-9451. DOI: 10.1007/s11235-015-0109-3.

[16] ALAM, T., M. R. I. FARUQUE and M. T. ISLAM. A corded shape printed wideband antenna design for multi-standard mobile applications. *Telecommunication Systems*. 2016, vol. 62, iss. 3, pp. 511–518. ISSN 1572-9451. DOI: 10.1007/s11235-015-0090-x.

[17] ZHI, N. C. and Y. W. C. MICHAEL. *Broadband planar antennas: design and applications*. Hoboken: John Wiley, 2006. ISBN 978-0-470-87174-4.

[18] WI, S.-H., Y.-S. LEE and J.-G. YOOK. Wideband Microstrip Patch Antenna With U-Shaped Parasitic Elements. *IEEE Transactions on Antennas and Propagation*. 2007, vol. 55, iss. 4, pp. 1196–1199. ISSN 1558-2221. DOI: 10.1109/TAP.2007.893427.

[19] ANSARI, J. A., A. MISHRA, N. P. YADAV, P. SINGH and B. R. VISHVAKARMA. Analysis of W-slot loaded patch antenna for dualband operation. *AEU - International Journal of Electronics and Communications*. 2012, vol. 66, iss. 1, pp. 32–38. ISSN 1434-8411. DOI: 10.1016/j.aeue.2011.04.011.

[20] VISHVAKARMA, S. and B. R. VISHVAKARMA. Analysis of inclined slot-loaded patch for dual-band operation. *Microwave and Optical Technology Letters*. 2006, vol. 48, iss. 12, pp. 2436–2441. ISSN 1098-2760. DOI: 10.1002/mop.21965.

[21] GOSALIA, K. and G. LAZZI. Reduced size, dual polarized microstrip patch antenna for wireless communications. *IEEE Transactions on Antennas and Propagation*. 2003, vol. 51, iss. 9, pp. 2182–2186. ISSN 1558-2221. DOI: 10.1109/TAP.2003.816344.

[22] MESHRAM, M. K. and B. R. VISHVAKARMA. Gap-coupled microstrip array antenna for wide-band operation. *International Journal of Electronics*. 2001, vol. 88, iss. 11, pp. 1161–1175. ISSN 1362-3060. DOI: 10.1080/00207210110071288.

[23] SHACKELFORD, A. K., K. F. LEE, K. M. LUK and R. C. CHAIR. U-slot patch antenna with shorting pin. *Electronic Letters*. 2001, vol. 37, iss. 12, pp. 729–730. ISSN 0013-5194. DOI: 10.1049/el:20010519.

[24] WONG, K.-L. and W.-S. CHEN. Compact microstrip antenna with dual-frequency operation. *Electronic Letters*. 1997, vol. 33, iss. 8, pp. 646–647. ISSN 0013-5194. DOI: 10.1049/el:19970433.

[25] PAN, S.-C. and K.-L. WONG. Dual-frequency triangular microstrip antenna with a shorting pin. *IEEE Transactions on Antennas and Propagation*. 1997, vol. 45, iss. 12, pp. 1889–1891. ISSN 1558-2221. DOI: 10.1109/8.650213.

[26] SINGH, A., M. ANEESH, K. KAMAKSHI, A. MISHRA and J. A. ANSARI. Analysis of F-shape microstrip line fed dualband antenna for WLAN applications. *Wireless Networks*. 2014, vol. 20, iss. 1, pp. 133–140. ISSN 1572-8196. DOI: 10.1007/s11276-013-0599-4.

[27] LEE, K. F., K. M. LUK, K. M. MAK and S. L. S. YANG. On the Use of U-Slots in the Design of Dual-and Triple-Band Patch Antennas. *IEEE Antennas and Propagation Magazine*. 2011, vol. 53, iss. 3, pp. 60–74. ISSN 1045-9243. DOI: 10.1109/MAP.2011.6028422.

[28] NEU, J.-X. Dual-band dual-mode patch antenna based on resonant-type metamaterial transmission line. *Electronic Letters*. 2010, vol. 46, iss. 4, pp. 266–268. ISSN 0013-5194. DOI: 10.1049/el.2010.3142.

[29] MISHRA, B., V. SINGH and R. SINGH. Dual and wide-band slot loaded stacked microstrip patch antenna for WLAN/WiMAX applications. *Microsystem Technologies*. 2017, vol. 23, iss. 8, pp. 3467–3475. ISSN 1432-1858. DOI: 10.1007/s00542-016-3120-z.

[30] SINGH, V., B. MISHRA, P. N. TRIPATHI and R. SINGH. A compact quad-band microstrip antenna for S and C-band applications. *Microwave and Optical Technology Letters*. 2016, vol. 58, iss. 6, pp. 1365–1369. ISSN 1098-2760. DOI: 10.1002/mop.29799.

[31] LIU, Y., Z. NIU and X. WANG. Dual-band H-shaped slot antenna for 2.4 and 5 GHz wireless communication. *Microwave and Optical Technology Letters*. 2010, vol. 52, iss. 4, pp. 957–959. ISSN 1098-2760. DOI: 10.1002/mop.25042.

[32] MURMU, S. K. and I. S. MISRA. Design of V-shaped microstrip patch antenna at 2.4 GHz. *Microwave and Optical Technology Letters*. 2011, vol. 53, iss. 4, pp. 806–811. ISSN 1098-2760. DOI: 10.1002/mop.25877.

[33] ASIF, S. M., A. IFTIKHAR, S. M. KHAN, M. USMAN and B. D. BRAATEN. An E-shaped microstrip patch antenna for reconfigurable dual-band operation. *Microwave and Optical Technology Letters*. 2016, vol. 58, iss. 6, pp. 1485–1490. ISSN 1098-2760. DOI: 10.1002/mop.29814.

[34] GU, J.-H., S.-S. ZHONG, L.-L. XUE and Z. SUN. Dual-band monopole antenna with L-shaped strips for 2.4/5 GHz WLAN applications. *Microwave and Optical Technology Letters*. 2008, vol. 50, iss. 11, pp. 2830–2833. ISSN 1098-2760. DOI: 10.1002/mop.23797.

[35] PANDA, J. R. and R. S. KSHETRIMAYUM. An F-shaped printed monopole antenna for dual-band RFID and WLAN applications. *Microwave and Optical Technology Letters*. 2011, vol. 53, iss. 7, pp. 1478–1481. ISSN 1098-2760. DOI: 10.1002/mop.26060.

[36] MARCUVITZ, N. *Waveguide handbook*. London: McGraw-Hill Book Company, 1986. ISBN 0-86341-058-8.

[37] CARVER, K. and J. MINK. Microstrip antenna technology. *IEEE Transactions on Antennas and Propagation*. 1981, vol. 29, iss. 1, pp. 2–24. ISSN 1558-2221. DOI: 10.1109/TAP.1981.1142523.

[38] KUMAR, G. and K. P. RAY. *Broadband microstrip antennas*. Boston: Artech House, 2003. ISBN 1-58053-244-6.

[39] MAEDA, M. An Analysis of Gap in Microstrip Transmission Lines. *IEEE Transactions on Microwave Theory and Techniques*. 1972, vol. 20, iss. 6, pp. 390–396. ISSN 1557-9670. DOI: 10.1109/TMTT.1972.1127768.

[40] GARG, R., P. BHARTIA, I. BAHL and A. ITTIPIBOON. *Microstrip antenna design handbook*. Boston: Artech House, 2001. ISBN 0-89006-513-6.

[41] SCHAUBERT, D. H., D. M. POZAR and A. ADRIAN. Effect of microstrip antenna substrate thickness and permittivity: comparison of theories with experiment. *IEEE Transactions on Antennas and Propagation*. 1989, vol. 37, iss. 6, pp. 677–682. ISSN 1558-2221. DOI: 10.1109/8.29353.

[42] POZAR, D. M. and S. M. DUFFY. A dual-band circularly polarized aperture-coupled stacked microstrip antenna for global positioning satellite. *IEEE Transactions on Antennas and Propagation*. 1997, vol. 45, iss. 11, pp. 1618–1625. ISSN 1558-2221. DOI: 10.1109/8.650073.

About Authors

Brijesh MISHRA was born in Azamgarh district of U.P. in 1988. He received B.Tech. degree in Electronic and Communication Engineering from Uttar Pradesh Technical University in 2010 and M.Tech. in Electronic Engineering from University of Allahabad in 2012. He has completed his Ph.D. degree from University of Allahabad recently in 2018. His research interests include design, simulation and fabrication of microwave devices and circuits and its applications. E-mail: brijesh.mishra0933@gmail.com

Vivek SINGH was born in Allahabad district of U.P. in 1987. He obtained his B.Tech. degree in Electronics & Communication Engineering from Uttar Pradesh Technical University in 2009 and M.Tech. in Electronics Engineering from University of Allahabad in 2012. Currently he is pursuing Ph.D. degree from University of Allahabad. His research interests include modelling and simulation of RF devices and circuits and its applications. E-mail: vivek.10singh@gmail.com

Rajeev SINGH was born in Azamgarh district of U.P. in 1968. He received B.Sc. degree in 1989, B.Tech. in Electronics & Telecommunications in 1992, M.Tech. in Electronics Engineering in 1994 all from University of Allahabad. He obtained his Ph.D.

degree in 2008 from University of Allahabad. He joined as Lecturer in the Department of Electronics and Communication, University of Allahabad in 1996, became Sr. Lecturer in 2002, Reader in 2007 and Associate Professor in 2010. He has received German Academic Exchange Service Fellowship (DAAD) in the year 2003. He has worked for his Ph.D. research work during DAAD fellowship in the University of Potsdam, Germany from June 2003 to December 2004. He again visited University of Potsdam in the year 2008 under re-invitation program of DAAD. His area of research is charge storing polymers, polymer electronics, photo stimulated charge profile measurements, thermal diffusivity of polymers, microwave and RF device and circuit simulation and its applications. E-mail: rsingh68@allduniv.ac.in, rsingh68@gmail.com